# Numerical Simulations of Liquid-Gas-Solid Three-Phase Flows in Microgravity

**Xinyu Zhang and Goodarz Ahmadi***
Department of Mechanical and Aeronautical Engineering, Clarkson University, Potsdam, N.Y. 13699—5725

Received: 15 August 2011, Accepted: 17 February 2012

**Abstract:**
Three-phase liquid-gas-solid flows under microgravity condition are studied. An Eulerian-Lagrangian computational model was developed and used in the simulations. In this approach, the liquid flow was modeled by a volume-averaged system of governing equations, whereas motions of particles and bubbles were evaluated using the Lagrangian trajectory analysis procedure. It was assumed that the bubbles remained spherical, and their shape variations were neglected. The bubble-liquid, particle-liquid and bubbl-particle two-way interactions were accounted for in the analysis. The discrete phase equations used included drag, lift, buoyancy, and virtual mass forces. Particle-particle interactions and bubble-bubble interactions were accounted for by the hard sphere model. Bubble coalescence was also included in the model. The transient flow characteristics of the three-phase flow were studied; and the effects of gravity, inlet bubble size and g-jitter acceleration on variation of flow characteristics were discussed. The low gravity simulations showed that most bubbles are aggregated in the inlet region. Also, under microgravity condition, bubble transient time is much longer than that in normal gravity. As a result, the Sauter mean bubble diameter, which is proportional to the transient time of the bubble, becomes rather large, reaching to more than 9 mm. The bubble plume in microgravity exhibits a plug type flow behavior. After the bubble plume reaches the free surface, particle volume fraction increases along the height of the column. The particles are mainly located outside the bubble plume, with very few particles being retained in the plume. In contrast to the normal gravity condition, the three phases in the column are poorly mixed under microgravity conditions. The velocities of the three phases were also found to be of the same order. Bubble size significantly affects the characteristics of the three-phase flows under microgravity conditions. For the same inlet bubble number density, the flow with larger bubbles evolves faster. The simulation results showed that the effect of g-jitter acceleration on the gas-liquid-particle three phase flows is small.

**Keywords:** Three-Phase, Gas-Liquid-Particle, Numerical Simulation, Eulerian-Lagrangian Method, Microgravity

## 1. INTRODUCTION

Three-phase flows with liquids, bubbles, and solid particles occur in many industrial processes (Fan, 1989). Important applications include three-phase slurry reactors in coal conversion processes (particularly in synthetic liquid fuel production). Optimization of three-phase slurry reactors requires a fundamental understanding of multiphase hydrodynamics coupled with heat and mass transfer processes. Despite a number of related studies, three-phase slurry reactor technology is far from being mature with many unresolved issues. In particular, the characteristics of three-phase flows under microgravity conditions are poorly understood. Three-phase slurry reactors, however, are expected to be a key component of air revitalization and air purification devices critical to NASA's plan for long duration human space travel.

Eulerian-Eulerian and Eulerian-Lagrangian approaches are common approaches for modeling multiphase flows. The Eulerian-Eulerian method is based on the concept of interpenetrating continua, where all the phases are treated as continuous media with properties analogous to those

*Corresponding Author:
Email address: gahmadi@clarkson.edu

of a fluid, while the Eulerian-Lagrangian approach adopts a continuum description for the liquid phase and tracks the discrete phases using Lagrangian particle trajectory analysis.

Applications of a number of Eulerian-Eulerian models were reported in the literature. For gas-particle flows, Ding and Gidaspow (1990) proposed a model for analyzing a bubbling fluidized bed using the kinetic theory of granular flows. Pita and Sundaresan (1993) carried out a numerical study on the developing flow of a gas-particle mixture in a vertical riser. Cao and Ahmadi (1995, 2000) studied gas-particle two-phase turbulent flows in vertical, horizontal and inclined ducts, where they accounted for the phasic fluctuation energy transport and interactions. For gas-liquid flows, Krishna et al. (1999) investigated the influence of scale on the hydrodynamics of bubble columns using an Eulerian-Eulerian model approach and a k-$\varepsilon$ turbulence model. Sanyal et al. (1999) simulated gas-liquid flows in a cylindrical bubble column using an Eulerian-Eulerian approach and compared their result with an algebraic slip mixture model. Borchers et al. (1999) described the applicability of the standard k-$\varepsilon$ turbulence model in an Eulerian- Eulerian approach for simulation of bubble columns. Mudde and Simonin (1999) performed their two- and three-dimensional simulations on a meandering bubble plume using the Eulerian-Eulerian method that included the k-$\varepsilon$ turbulence model.

An Eulerian-Eulerian approach requires development of empirical constitutive equations and the accuracy of the model predictions depends on the accuracy of the correlations used. In addition, the Eulerian-Eulerian approach has certain limitations for predicting some of the discrete phase characteristics, such as particle size effect, particle agglomeration and bubble breakup and coalescence. The Eulerian-Lagrangian model, however, involves a smaller number of empirical equations and is more suitable for providing detailed information on the discrete phase properties. These advantages are at the expense of the more extensive computing time requirement for the Eulerian-Lagrangian approach.

The Eulerian-Lagrangian model has been widely used in two-phase flows. Li et al. (1994) and Kvasnak and Ahmadi (1996) studied particle transport and deposition in duct flows and included a model for the instantaneous turbulent velocity field using an anisotropic Gaussian random field model. Tsuji et al. (1993) conducted a discrete particle simulation of a two-dimensional fluidized bed with a soft particle model. Their model was further modified by Hoomans et al. (1996) and Xu and Yu (1997) who developed hard sphere collision models. Zhang (1998) carried out a simulation of gas-particle flows in curved ducts using particle-wall and particle-particle random impact models. Patankar and Joseph (2001a, b) performed simulations of particulate flows using a Chorin-type fractional-step method for gas phase equations. Fan et al. (2001) performed simulations of particle dispersion in a three-dimensional temporal mixing layer. They found that the particle dispersion patterns were governed by the large-scale vortex structures. Using the DNS method, Fan et al. (2003) studied particle modulation on coherent vortex structures. Fan et al. (2004) also studied a near-field particle-laden plane turbulent jet. Recently Mansoori et al. (2002a, b) analyzed gas-solid flows in a duct using a four-way interaction approach including the particle-particle collision and heat transfer.

An Eulerian-Lagrangian approach for bubbly flows was used by Webb et al. (1992), Trapp and Mortensen (1993), Lapin and Lubbert (1994), and Devanathan et al. (1995). Neglecting bubble-bubble interactions, Sokolichin et al. (1997) compared the simulation results of their Eulerian-Eulerian model and Eulerian-Lagrangian model with the experimental data. Delnoij et al. (1997a, b) reported an Eulerian-Lagrangian model for a bubble column operating in the homogeneous flow regime. Their simulations included bubble-bubble interactions using a collision model, but neglected bubble coalescence. Lain et al. (1999, 2002) reported an Eulerian-Lagrangian approach including turbulence effect using the k-$\varepsilon$ model, but they neglected the effect of phase volume fractions. More recently, ignoring bubble-bubble interactions, Lapin et al. (2002) provided their Eulerian-Lagrangian simulations for slender bubble columns. Their prediction suggests that the flow moves downwards near the axis and rises close to the wall in the lower part of the column, but in the upper part the opposite trend is found.

Studies on three-phase liquid-gas-solid flow hydrodynamics are rather scarce. Gidaspow et al. (1994) developed a model for three-phase slurry hydrodynamics. Grevskott et al. (1996) described a two-fluid model for three-phase bubble columns in cylindrical coordinates. They used a k-$\varepsilon$ turbulence model and included bubble-generated turbulence. Mitra-Majumdar et al. (1997) provided a computational fluid dynamic (CFD) model for examining the structure of three-phase

flows through a vertical column. They proposed new correlations for the drag between the liquid and the bubbles and included the particle effects on bubbles motions. Wu and Gidaspow (2000) simulated a gas-liquid slurry bubbly flow using the kinetic theory of granular flows for particle collisions. Padial et al. (2000) reported simulations of three-phase flows in a three-dimensional draft-tube bubble column using a finite-volume technique. Gamwo et al. (2003) developed a CFD model for a chemically active three-phase slurry reactor for methanol synthesis. Zhou et al. (2005) reported a second-order moment three-phase turbulence model for simulating gas-liquid-solid flows. However, all these models were based on an Eulerian-Eulerian approach. Computer simulations of gas-liquid-solid flows using an Eulerian-Lagrangian model are also rather scarce. Zhang (1999) performed a series of simulations of three- phase flow using a volume-of-fluid (VOF) method for the liquid and gas phases and a Lagrangian method for particles. His study, however, was limited to consideration of only a small number of bubbles. Recently Bourloutski and Sommerfeld (2002) reported their simulations on dense gas-liquid-solid flows using the standard k-$\varepsilon$ turbulence model, without considering bubble coalescence, bubble-bubble collision or particle-particle collision.

Recently, Zhang and Ahmadi (2005) developed a computational model for simulations of gas-liquid-solid flows, where the bubbles and particles were treated as the dispersed discrete phases and their motions were simulated by the Lagrangian trajectory analysis procedure. Two-way coupling between the continuous liquid phase and the particles and bubbles were accounted for, and interactions between particle-particle, bubble-bubble, and particle-bubble as well as bubble coalescence were also included. Their simulation results were in agreement with the experimental data of Delnoij et al. (1997a). In this study the computational model developed earlier was used. While the study was focused on the zero-gravity case, a sample case with normal gravity was also analyzed. The transient characteristics of three-phase flows were studied, and the effects of gravity, bubble size and g-jitter acceleration under microgravity condition were analyzed.

## 2. GOVERNING EQUATIONS AND MODELS

Details of governing equations and model assumptions were described by Zhang and Ahmadi (2005). Therefore, here an outline of the key equations is presented.

### 2.1. Fluid Phase Hydrodynamics

The liquid phase is described by volume-averaged, incompressible, transient Navier-Stokes equations. The volume-averaged continuity and momentum equations are given as

$$\frac{\partial(\varepsilon_f \rho_f)}{\partial t} + \nabla \cdot (\varepsilon_f \rho_f \mathbf{u_f}) = 0, \tag{1}$$

$$\rho_f \varepsilon_f \frac{d(\mathbf{u_f})}{dt} = -\varepsilon_f \nabla p + \nabla \cdot (\varepsilon_f \boldsymbol{\tau}_\mathbf{f}) + \rho_f \, \mathbf{g} \varepsilon_f + \mathbf{P}. \tag{2}$$

Here $\varepsilon_f$ is the liquid phase volume fraction, $\rho_f$ is the liquid phase density, $\mathbf{u_f}$ is the fluid phase average velocity, $p$ is pressure, $\mathbf{g}$ is the acceleration of gravity, $\mathbf{P}$ is interaction momentum supply per unit mass transferred from the discrete phases, and $\tau_\mathbf{f}$ is the liquid phase viscous stress tensor, which is assumed to obey the general Newtonian fluid form given as

$$\boldsymbol{\tau}_\mathbf{f} = -\frac{2}{3}\mu_f \left(\nabla \cdot \mathbf{u_f}\right) I + \mu_f \left( \left(\nabla \mathbf{u_f}\right) + \left(\nabla \mathbf{u_f}\right)^T \right), \tag{3}$$

where $\mu_f$ is the liquid viscosity.

### 2.2. Dispersed Phase Dynamics

The bubbles and particles are treated as discrete phases, and their motions are governed by Newton's second law:

$$m_d \frac{d\mathbf{u_d}}{dt} = \mathbf{F_d} + \mathbf{F_b} + \mathbf{F_{vm}} + \mathbf{F_l} + \mathbf{F_{Int}}. \tag{4}$$

Here $m_d$ and $\mathbf{u_d}$ are, respectively, mass and the discrete phase velocity. The terms on the right hand side of Equation (4) are, respectively, drag, buoyancy, virtual mass, lift and interaction forces. Here the interaction force $\mathbf{F_{Int}}$ includes particle-particle, bubble-bubble and particle-bubble collisions.

The drag force, $\mathbf{F_d}$, is given by

$$\mathbf{F_d} = \begin{cases} 0.125\rho_f C_D \pi d_d^2 \left|\mathbf{u_f} - \mathbf{u_d}\right|\left(\mathbf{u_f} - \mathbf{u_d}\right), & \mathrm{Re}_d \geq 1 \\ \alpha_d \pi \mu_f d_d \left(\mathbf{u_f} - \mathbf{u_d}\right), & \mathrm{Re}_d < 1 \end{cases} \tag{5}$$

where $d_d$ is the discrete phase diameter, $\alpha_d$ is a phase coefficient whose value is 2 for bubble and 3 for rigid particle to account for the variation of the Stokes drag force for bubbles and particles in low Reynolds number flows. In Equation (5), $\mathrm{Re}_d$ is the discrete phase Reynolds number defined as

$$\mathrm{Re}_d = \rho_f d_d \frac{\left|\mathbf{u_f} - \mathbf{u_d}\right|}{\mu_f}, \tag{6}$$

and $C_D$ is the drag coefficient given by

$$C_D = f_d \frac{24}{\mathrm{Re}_d}. \tag{7}$$

Here, $f_d$ is given by

$$f_d = \begin{cases} 1 + 0.15\,\mathrm{Re}_d^{0.687}, \mathrm{Re}_d \leq 1000 \\ 0.0183\,\mathrm{Re}_d, \mathrm{Re}_d > 1000 \end{cases}. \tag{8}$$

In Equation (4), $\mathbf{F_l}$ is the Saffman lift force given by

$$\mathbf{F_l} = 1.61 d_d^2 \left(\mu_f \rho_f\right)^{0.5} \left|\boldsymbol{\omega_f}\right|^{-0.5} \left[\left(\mathbf{u_f} - \mathbf{u_d}\right) \times \boldsymbol{\omega_f}\right], \tag{9}$$

where flow vorticity $\omega_\mathbf{f}$ is defined as

$$\boldsymbol{\omega_f} = \nabla \times \mathbf{u_f}. \tag{10}$$

Similarly, $\mathbf{F_b}$ is the buoyancy force given by

$$\mathbf{F_b} = \frac{\pi d_d^3}{6}(\rho_f - \rho_d)\mathbf{g}, \tag{11}$$

where $\rho_d$ is the discrete phase density. In Equation (4), $\mathbf{F_{vm}}$ is the virtual mass force given as

$$\mathbf{F_{vm}} = -\frac{1}{12}\pi d_d^3 \rho_f \frac{d}{dt}\left(\mathbf{u_d} - \mathbf{u_f}\right). \tag{12}$$

### 2.3. Discrete Phase Collisions and Two-Way Coupling

Bubble-bubble and particle-particle collisions are considered in this study by using a hard sphere collision model along the line of the model developed by Hoomans et al. (1996). However, in the analysis, the effects of the rotation of bubbles and particles were neglected. Restitution coefficients of 0.2 and 0.5 are used for bubble-bubble and particle-particle collisions, respectively. Friction coefficients of 0.02 and 0.1 are assumed for bubbles and particles, and all the bubble-bubble and particle-particle collisions are assumed to be binary collisions.

Bubble-particle interactions are accounted for in the analysis by assuming the particles always go through the bubbles when bubble-particle collision occurs. Unlike bubble-bubble and particle-particle collisions, which are assumed to be binary collisions, multi-interactions between bubble and particle are accounted for in this model; therefore, more than one particle can enter a bubble at the same time. In the present study, bubble coalescence is accounted for by assuming that two bubbles coalesce upon impact when the Weber number is less than 0.14, while they bounce for larger Weber numbers.

Two-way coupling is included in the model. The coupling between fluid and dispersed phases is implemented through the momentum interaction term **P** in Equation (2). In this equation, **P** is the negative of the sum of all forces acting on the particles and bubbles from the liquid in a certain Eulerian cell. The coupling between bubbles and particles is implemented through bubble-particle interactions. When a particle enters a bubble, all the forces acting on the particles by the new gaseous environment are calculated using the bubble's (air) hydrodynamic properties until the particle leaves the bubble. The exact force with opposite direction is then added to the bubble's equation of motion.

### 2.4. Geometry and Boundary Conditions

In the present study, a pseudo-two-dimensional bubble column with a rectangular cross-section is considered. Figure 1 shows the schematics of the bubble column. The column is 25 cm wide, 75 cm high and 2 cm thick. The gas is injected from 14 uniformly spaced gas inlets located in the center of the bottom of the column. The distance between every two neighboring inlets is 4mm. In the simulations, neutrally buoyant particles were randomly distributed in the column at the initial time. The continuous phase was assumed to be liquid water. The physical properties of water were kept fixed in the simulations, and the initial liquid level was assumed to be 55 cm high, while the gravity as well as the bubble's initial diameter and superficial velocity were varied for different cases. Table 1 summarizes the hydrodynamic properties of the dispersed phases for different cases studied. The study was focused on the comparison of the three-phase flows in the bubble column in microgravity and normal gravity conditions.

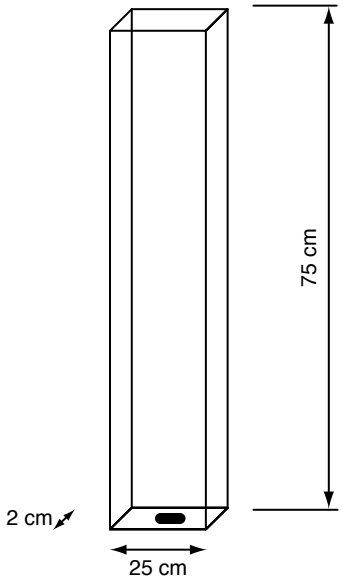


Figure 1: Schematics of the pseudo-two-dimensional bubble column.

**Table 1. Hydrodynamic parameters for different cases.**

| Case number | Bubble diameter mm | Superficial gas velocity mm/s | Bubble density kg/m$^3$ | Particle diameter mm | Particle density kg/m$^3$ | Gravity m/s$^2$ |
|---|---|---|---|---|---|---|
| 1 | 1.0 | 0.25 | 1.29 | 0.25 | 1000 | –9.8 |
| 2 | 1.0 | 0.25 | 1.29 | 0.25 | 1000 | 0.0 |
| 3 | 3.0 | 6.75 | 1.29 | 0.25 | 1000 | 0.0 |
| 4 | 3.0 | 6.75 | 1.29 | 0.25 | 1000 | G-jitter |

No-slip boundary conditions were imposed on three walls of the column for the liquid phase, and an outflow condition was assumed at the upper boundary of the column. Bubble-wall and particle-wall collisions were accounted for in the model by the hard sphere collision model adopted from the model developed by Hoomans et al. (1996). The wall roughness effects and the rotation of bubbles and particles were neglected. A restitution coefficient of 0.5 was used for both bubble-wall collisions and particle-wall collisions. Similarly, friction coefficients of 0.02 and 0.1 were assumed for bubble-wall collision and particle-wall collision, respectively.

The marker-and-cell (MAC) method (Harlow and Welch, 1965) was used to simulate the column's free surface. A simple hard sphere model accounting for interaction of bubbles with the free surface was used in the simulation. It was assumed that the bubbles that impact the column's free surface with a Weber number less than 0.28 will break and leave the column, while bubbles impacting at higher Weber numbers will bounce. A restitution coefficient of 0.2 was used for bubble-free surface collisions for We > 0.28. Additional details of the boundary conditions used for the free surface were described by Zhang and Ahmadi (2005).

### 2.5. Numerical Procedure

The governing equations of the model were discretized using the finite difference method for a structured equidistance staggered grid. A central and upwind (donor cell) discretization scheme was used for convective parts, while an explicit time step was used for time updating. The model was implemented in a newly developed computer code ELM3PF (Eulerian-Lagrangian Method for Three-Phase Flow) for simulation of three- phase flows. The new code uses C and is based on NaSt2D code, which is a code for single-phase flows with free surface developed by Griebel et al. (1998). ELM3PF code can simulate unsteady, two-dimensional three-phase liquid-gas-solid flows with free surface.

ELM3PF solves the Poisson equation for liquid-phase pressure by the successive over-relaxation (SOR) method. A fixed time step, $\Delta t$ (typically 0.001s), is used to evaluate the updated liquid phase velocity field in the column first. The code then evaluates the minimum time dt for the next collision of all possible collisions. If dt is smaller than $\Delta t$, the code computes the bubble and particle velocities and positions over the time duration dt. The next collision process is then analyzed, and the corresponding discrete phase velocities after the collision are evaluated. Then the code computes the next minimum time for collision and repeats this procedure until the accumulation of these dt's equals $\Delta t$. At this point, the forces acting on the bubbles and particles are evaluated, and the corresponding momentum supply term is added to the momentum equation for the liquid phase at appropriate grid points. The code then computes the new liquid velocity field. If the minimum collision time dt is larger than $\Delta t$, the code computes the forces acting on the bubbles and particles, and then transfers the corresponding momentum supply term to the momentum equations for liquid phase and evaluates the new liquid velocity field. The time marching process continues until the desired time duration is covered. In the present study, typically, 9940 bubbles and 1000 particles are used. The CPU time requirement depends on the number of particles, bubbles and grid cells. For a typical number of bubbles and particles with a computational grid of 1500 cells, evaluation of one second transient behavior of the liquid-gas-solid three-phase flow requires around 4 hours of CPU time on a SUN Ultra10 workstation.

### 2.6. Effect of Grid Size

To check the sensitivity of the simulation results to the grid size, the grid spacing was reduced by a factor of two from 1 cm to 0.5 cm. The results for the two cases did not show a noticeable difference in the simulation results. Thus, a grid spacing of 1 cm was typically used for the sake of computational economy.

## 3. RESULTS AND DISCUSSION

### 3.1. Development of Transient Flow Structures with Normal Gravity

To study the effect of gravity on the flow characteristics, a sample reference case with normal gravity is first presented. The hydrodynamic parameters used in the simulation are listed in Table 1 (case 1). Figure 2 shows the snapshots of the model predictions for the liquid stream traces and the locations of bubbles and particles at times of 1, 9, 22 and 30 s after initiation of the flow. In Figure 2, the small dots show the liquid phase stream traces, while the small circles and the large circles show, respectively, the positions of the particles and the bubbles. This figure shows the evolution of the flow structure in the bubble column. Figures 3, 4 and 5 show, respectively, the corresponding bubble velocities, liquid velocities and particle velocities at different times. The transient characteristics of the three-phase flow can clearly be seen from these figures. In the first 22 s, the bubble plume rises rectilinearly along the centerline of the column, which generates two vortices behind the plume head. These vortices are almost symmetric in the first 22 s, but with the further development of the bubble plume, the vortices become non-symmetric. As seen from Figure 4d, staggered vortical flows eventually form in the column. As a result, the bubble plume changes its path to the S-shape that can be seen in Figure 2d. With the upward flow of the bubble plume, these staggered vortices move downward and result in an oscillation of the bubble plume. Figure 4 also shows that the liquid velocities generated by the counter-rotating vortices in the bottom of the column point toward the center of the column. This tends to move the bubbles toward the centerline, and thus the bubble plume shrinks in this region. On the column top, however, an opposite trend exists that drags the bubbles toward the column walls. As a result, the head of the bubble plume expands, as is seen in Figure 2. Comparing Figures 2 and 4 shows that the evolution of the three-phase flow in the column is controlled by these time-dependent staggered vortices.

Figures 2, 4 and 5 show solid particles are mainly concentrated in the region outside the large vortices. This is due to the effect of the centrifugal force that tends to move the particles away form the center of the vortices. Some particles are retained inside these staggered vortices, partly due to particle-particle collisions.

Figures 2, 3 and 4 reveal that a number of bubbles are captured by the staggered vortices and move with the vortices as is seen from Figures 2c, 2d, 3c, 3d, 4c and 4d. In general, these captured

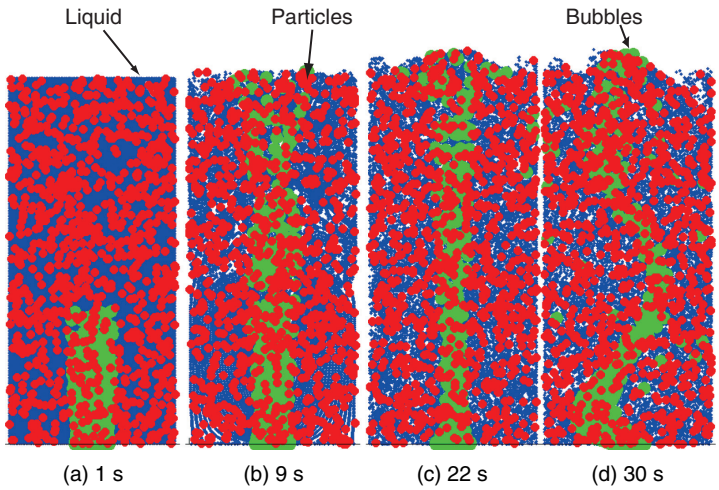


Figure 2: Computed flow structure of the gas-liquid-particle three-phase flow under normal gravity. Superficial gas velocity, $U_s$ = 0.25 mm/s, initial bubble size, $d_b$ = 1.0 mm, particle size, $d_p$ = 0.25 mm.

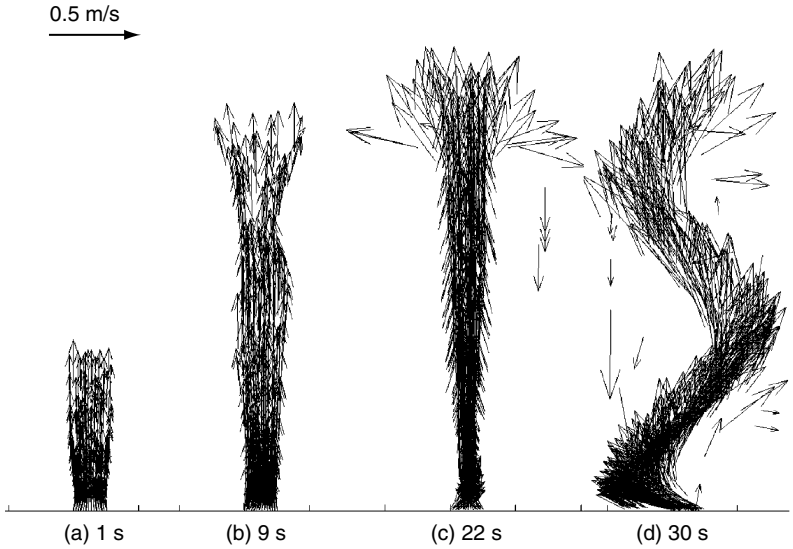


Figure 3: Computed snapshots of the bubble velocities of the gas-liquid-particle three-phase flow under normal gravity. Superficial gas velocity, $U_s$ = 0.25 mm/s, initial bubble size, $d_b$ = 1.0 mm, particle size, $d_p$ = 0.25 mm.

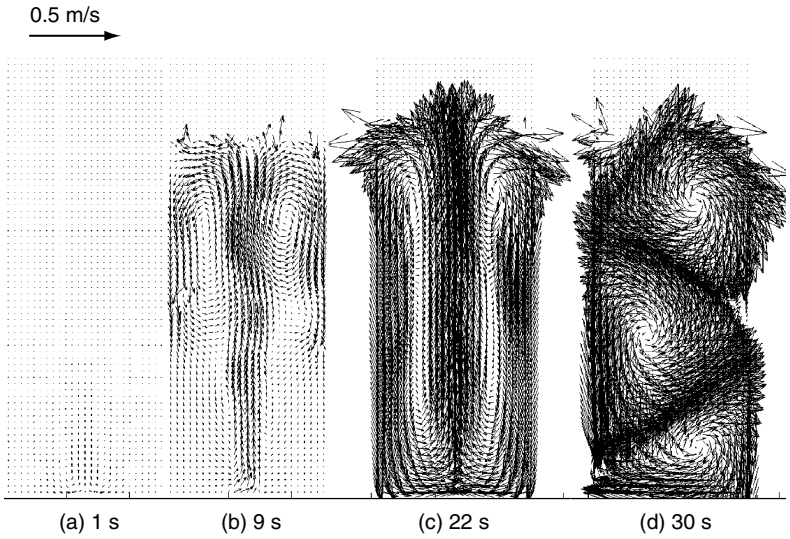


Figure 4: Computed snapshots of the liquid velocities of the gas-liquid-particle three-phase flow under normal gravity. Superficial gas velocity, $U_s$ = 0.25 mm/s, initial bubble size $d_b$ = 1.0 mm, particle size $d_p$ = 0.25 mm.

bubbles are at some distance from the center of the vortices. Similarly, Figures 2, 4 and 5 show that some particles are also captured by the vortices and are carried around by the time-dependent circulating motions. Comparison of Figures 3, 4 and 5 indicates that the bubble upward velocities are much larger than both particle and liquid velocities, but bubble downward velocities are smaller than the other phase velocities.

Figures 4 and 5 show that the magnitudes of particle and liquid velocities are of the same order, with particle downward and upward velocities being somewhat smaller than that of liquid. In some regions, however, particle upward velocities can be slightly larger than the liquid velocities. In general, the differences between the liquid and particle velocities are very small.

The observed velocity characteristics of the three-phase flow can be explained by the effect of the bubble buoyancy force, particle inertia and liquid viscosity. The bubble buoyancy is the main

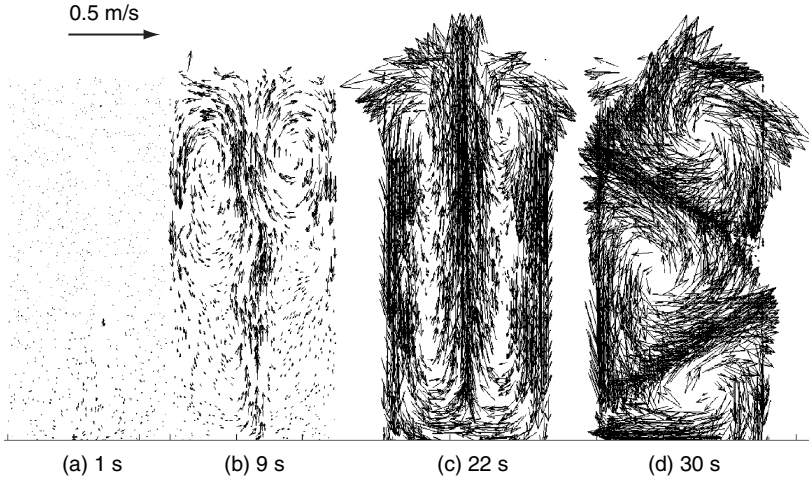


Figure 5: Computed snapshots of the particle velocities of the gas-liquid-particle three-phase flow under normal gravity. Superficial gas velocity, $U_s$ = 0.25 mm/s, initial bubble size, $d_b$ = 1.0 mm, particle size, $d_p$ = 0.25 mm.

driving force for the flow under normal gravity condition. The bubble drags the liquid and the particles upwards along its time-evolving S-shape path. Thus, bubble upward velocities in the column are larger than both liquid and particle velocities. While in the regions outside the staggered vortices, the liquid velocity is downward, and the drag of liquid on the bubbles is also downward. However the bubble buoyancy force is upward, so the bubble can not follow the liquid closely. Therefore, in this region the bubble velocities are smaller than both particle and liquid velocities.

Because the neutrally buoyant particles are generally transported by the liquid, the particle velocity is slightly smaller than the liquid velocity. However, particles with high velocities may entrain in the low liquid velocity region; in these situations, the particle local velocities may become slightly larger than the liquid phase.

Figures 6 and 7 show, respectively, average volume fractions of the bubbles and particles along the column height. Here, a and b refer to the time periods 5–20 s and 20–30 s, respectively. As expected, comparison of Figure 6a and 6b indicates that the bubble volume fraction increases with time. The reason is that as time increases, the number of gas bubbles in the S-shape plume increases. In addition, the air volume fraction in the separated bubbles also increases. Figure 6 also

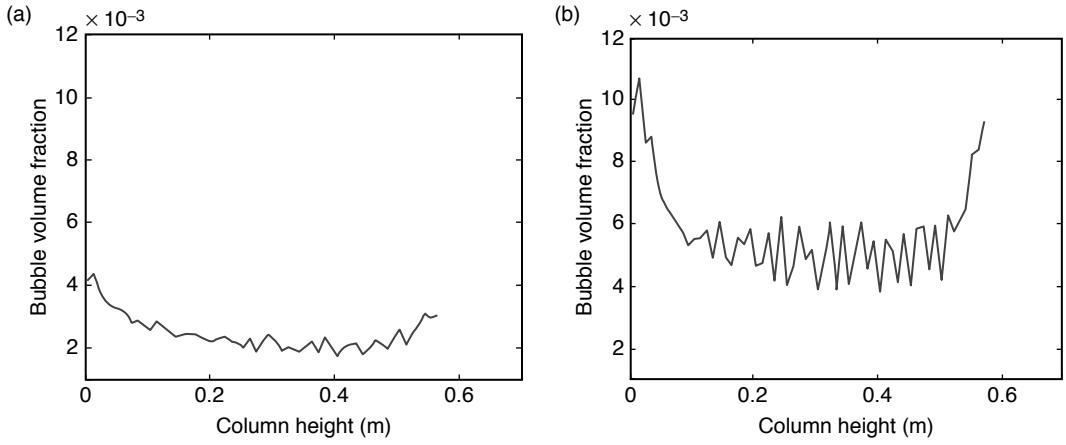


Figure 6: Average volume fraction of the bubbles along the column height during gas-liquid-particle three-phase flows under normal gravity. Superficial gas velocity, $U_s$ = 0.25 mm/s, initial bubble size $d_b$ = 1.0 mm, particle size $d_p$ = 0.25 mm. (a) Averaged over 5—20 s (b) Averaged over 20—30 s.

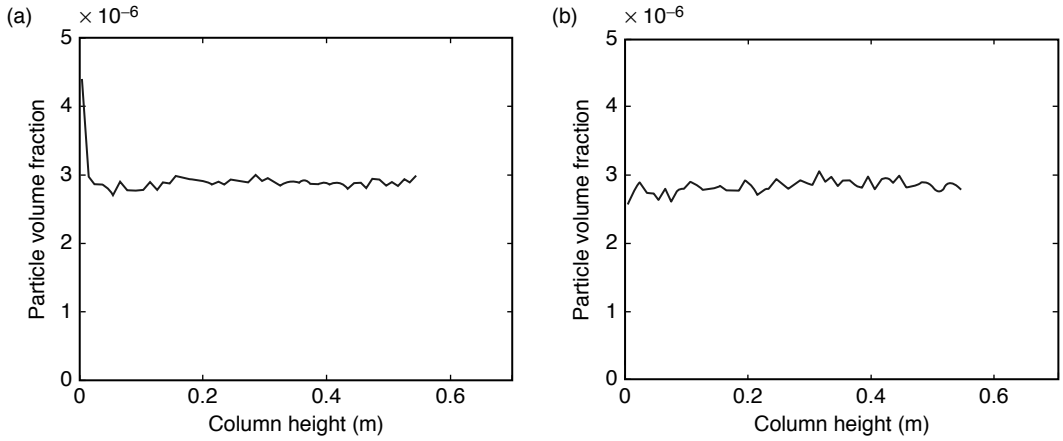


Figure 7: Average volume fraction of the particles along the column height during gas-liquid-particle three-phase flow under normal gravity. Superficial gas velocity, $U_s$ = 0.25 mm/s, initial bubble size $d_b$ = 1.0 mm, particle size $d_p$ = 0.25 mm. (a) Averaged over 5—20 s (b) Averaged over 20—30 s.

shows that, along the height of column, bubble volume fraction at the bottom is highest; it decreases as it reaches its minimum value at about the two-thirds up the height of the column, and then increases toward the column top. This trend may be explained by the variation of bubble upward velocity in the column. As seen from Figure 3c and 3d, bubble upward velocity increases along the column, attains its maximum at about two-thirds up the column height, and then decreases along the column height toward the free surface. A larger bubble upward velocity implies a shorter residence time, and leads to lower bubble volume fraction. Another reason for the observed bubble volume fraction profile could be the result of the presence of staggered vortices in the column.

Figure 7 shows the variation of the particle volume fraction in the column. For the time duration of 5–20 s, Figure 7a shows that the particle concentration is roughly constant except for a relatively high peak near the bottom of the column. As seen from Figures 4a and 4b, at the initial state of flow development, the liquid velocity near the bottom of the column is not very large. The particles are transported by the downward liquid velocities and collide with the bottom wall of the column. These particles lose their momentum and stay near the wall. As a result, the particle volume fraction in the region near the bottom wall is high. However, with the further development of the flow, the horizontal liquid velocities near the bottom wall become sufficiently high and move the near wall particles to the central part of the column. The particles are then captured by the upward flow generated by the bubble plume. As a result, for the 20–30 s time period, the high particle volume fraction in the region near the bottom disappears; Figure 7b shows a roughly uniform particle volume fraction along the column height.

Figures 8a and 8b, respectively, show the average Sauter mean diameter of the bubbles along the column height for time periods of 5–20 s and 20–30 s. These figures indicate that the bubble diameter increases with the column height and the time evolution of the flow. Clearly, the longer the bubbles reside in the column, the higher the possibility they will collide with each other and coalesce. Thus, bubble diameter increases along the column height due to bubble coalescence. The bubble diameter increases with the time evolution of the flow not only because the developed S-shape plume traps the bubbles, but also because formed staggered vortices generate strong disturbances, which increase bubble-bubble collisions and coalescences.

Figures 9a and 9b show average bubble size distribution in the entire column for periods 5–20 s and 20–30 s, respectively. These figures show that the 1–2 mm bubbles have the largest number density and the number density decreases as the size increases. As noted before, the initial bubble diameter is 1 mm, and due to bubble coalescence larger size bubbles are formed. Comparison of Figures 9a and 9b indicates that with the time development of the flow, the number density of small bubbles decreases and the number density of large bubbles increases.

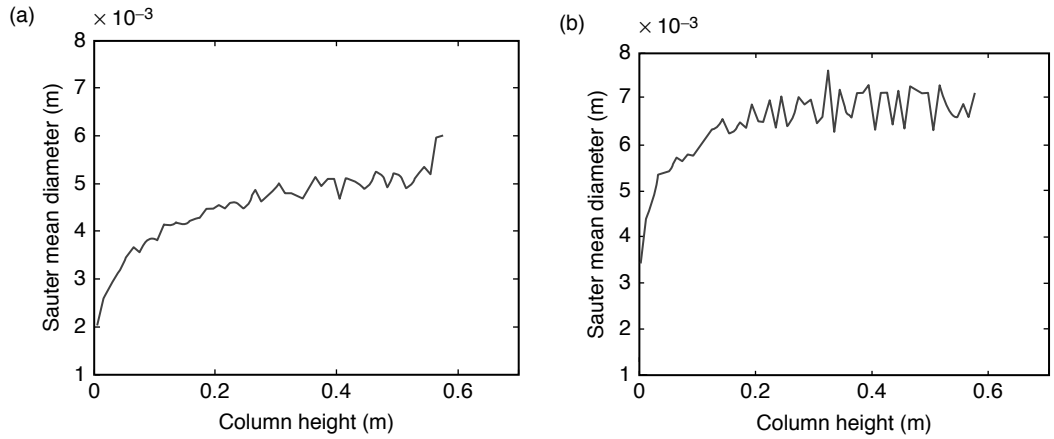


Figure 8: Average Sauter mean diameter of the bubbles along the column height in the gas-liquid-particle three-phase flow under normal gravity. Superficial gas velocity $U_s$ = 0.25 mm/s, initial bubble size $d_b$ = 1.0 mm, particle size $d_p$ = 0.25 mm. (a) Averaged over 5—20 s. (b) Averaged over 20—30 s.

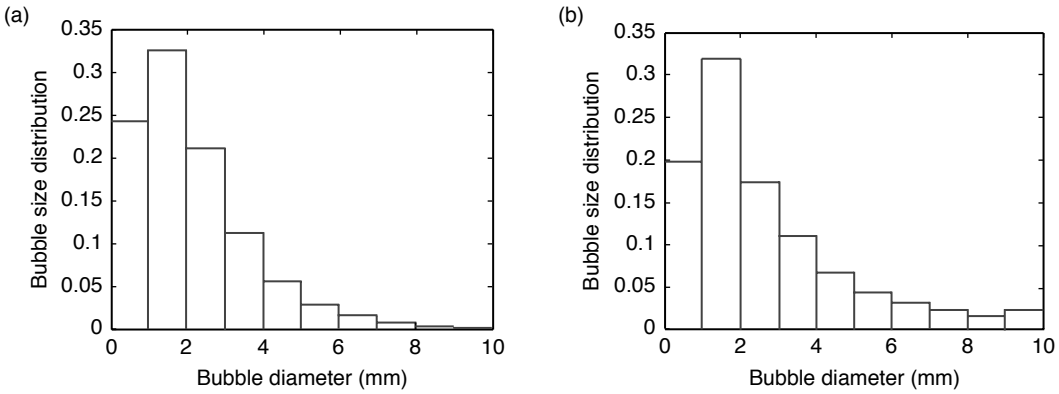


Figure 9: Average bubble size distribution during the gas-liquid-particle three-phase flow under normal gravity in the entire column. Superficial gas velocity, $U_s$ = 0.25 mm/s, initial bubble size, $d_b$ = 1.0 mm, particle size $d_p$ = 0.25 mm. (a) Averaged over 5—20 s. (b) Averaged over 20—30 s.

### 3.2. Development of Transient Flow Structures under Zero-Gravity Condition

Characteristics of the three-phase liquid-gas-solid flows under zero-gravity condition are studied in this section. The hydrodynamic parameters used in the simulation are listed in Table 1 (case 2). Figure 10 shows the snapshots of the model predictions for the liquid stream traces and the locations of bubbles and particles at the time of 5, 10, 15 and 20 s after initiation of the flow. Figures 11, 12 and 13 show the corresponding bubble velocities, liquid velocities and particle velocities, respectively,. The transient characteristics and the development of the three-phase flow are clearly shown in these figures. In the absence of gravity, there is no buoyancy force acting on the bubbles or the particles. Bubble motions are then due to the bubble initial injection momentum, bubble-bubble collisions, bubble-particle collisions, and liquid drag. Thus, compared to the flow with normal gravity, bubbles move very slowly in the column under zero-gravity condition.

Unlike the case for normal gravity, Figure 10a shows that bubbles do not rise rectilinearly under zero-gravity condition. When bubbles enter the column, they quickly lose their initial momentum due to the liquid drag, and they then accumulate at the bottom of the column due to the lack of buoyancy force. After a certain time when a sufficient number of bubbles is reached, they begin to rise due to bubble-bubble collision and liquid motion. Figures 11a and 12a show that the movements of the bubble clusters are along the liquid vertical path. Figures 10a and 13a show that

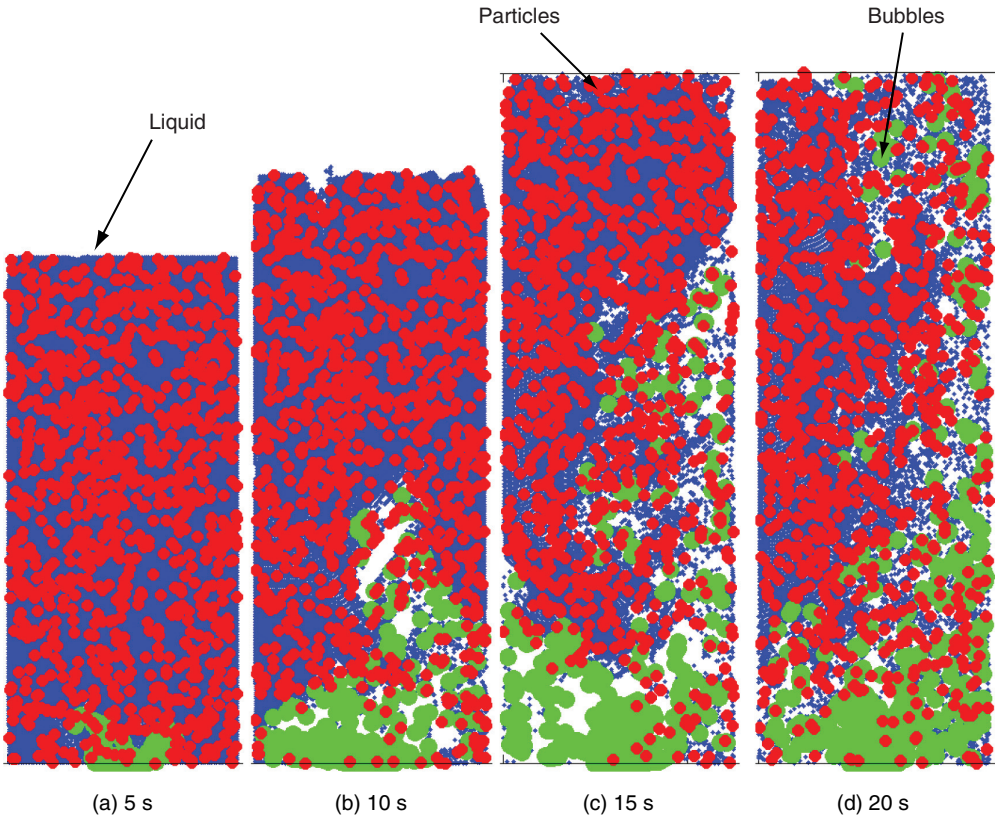


Figure 10: Computed flow structure of the gas-liquid-particle three-phase flows in zero-gravity. Superficial gas velocity $U_s$ = 0.25 mm/s, initial bubble size, $d_b$ = 1.0 mm, particle size, $d_p$ = 0.25 mm.

particles are pushed away when the bubble clusters are raised. Figures 10b and 10c show the significant increase of the liquid level in the column with time, which is the result of the accumulation of a large number of bubbles in the column in zero-gravity condition. Figures 10b, 11b, and 12b show a plug flow behavior in the bubble column with the liquid above the bubble clusters moving with a roughly uniform velocity. When the bubble plume reaches the free surface, Figures 10d, 11d and 12d show that a large vortex is formed in the column. Figures 10 and 13 also show that particles are mainly located outside the bubble plume, with only a few particles retained inside the plume.

Comparison of Figures 11, 12 and 13 indicates that, except for the startup when the bubble upward velocities are much larger than both liquid and particle velocities, the velocities of bubbles, liquid and particles are of the same order under the zero-gravity condition, especially at the top of the column. At the bottom of the column, bubbles push the liquid, and the liquid transports the particles; thus the bubble velocity is somewhat larger, and the particle velocity is slightly smaller.

Comparing Figures 10, 11, 12 and 13, respectively, with Figures 2, 3, 4 and 5 for the normal gravity, shows the significant effect of gravity on the three-phase flow characteristics in the column. Clearly, bubble rising velocities are very low due to the lack of buoyancy force. Also because of bubble accumulation in the column, the liquid level in the column at zero-gravity is much higher than that of the flow with normal gravity. In addition, most particles are located outside the bubble plume; as a result, the mixing of different phases is much less when compared with that for the flow with normal gravity. Thus, the interactions among the different phases are significantly reduced in zero-gravity condition. Compared to Figures 4 and 5, Figures 12 and 13 show that both liquid and particle velocities are smaller than those of the flow with normal gravity. In summary, compared with the flow in normal gravity, the flow in zero-gravity has low phase velocity and phase mixing.

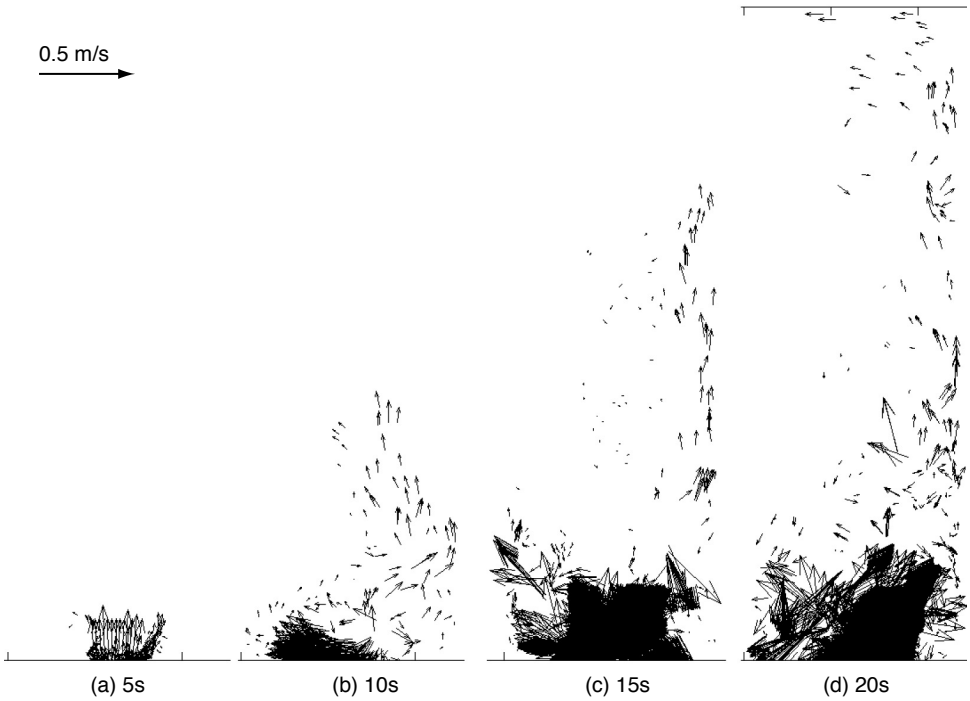


Figure 11: Computed snapshots of the bubble velocities of the gas-liquid-particle three phase flows in zero-gravity. Superficial gas velocity, $U_s$ = 0.25 mm/s, initial bubble size, $d_b$ = 1.0 mm, particle size, $d_p$ = 0.25 mm.

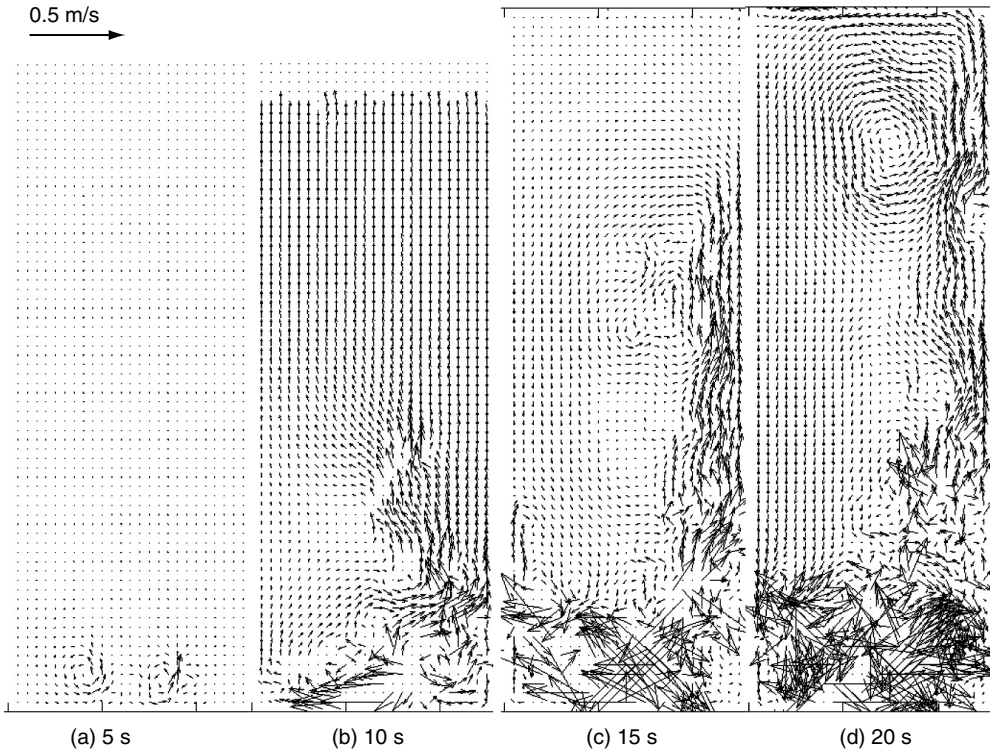


Figure 12: Computed snapshots of the liquid velocities of the gas-liquid-particle three-phase flow in zero-gravity. Superficial gas velocity, $U_s$ = 0.25 mm/s, initial bubble size $d_b$ = 1.0 mm, particle size, $d_p$ = 0.25 mm.

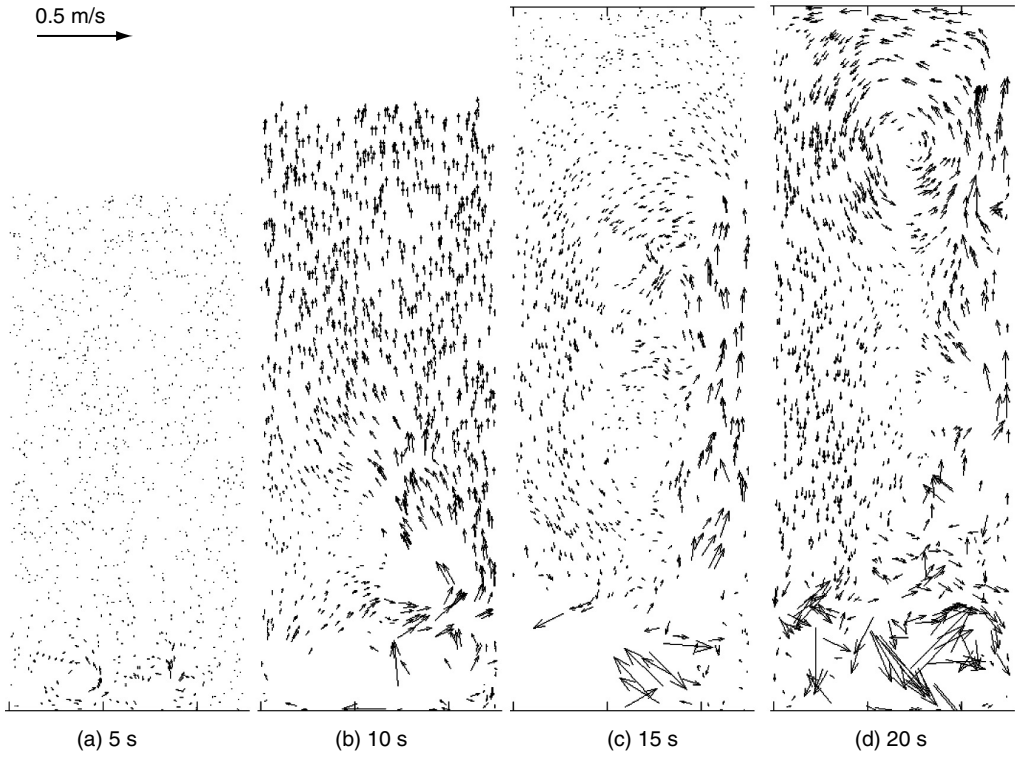


Figure 13: Computed snapshots of the particle velocities of the gas-liquid-particle three-phase flow in zero-gravity. Superficial gas velocity, $U_s$ = 0.25 mm/s, initial bubble size $d_b$ = 1.0 mm, particle size $d_p$ = 0.25 mm.

Figures 14 and 15 show, respectively, the average volume fractions of bubbles and particles along the column height during three-phase flows under zero-gravity condition. Here, a and b refer to the time averaging periods from 5 to 20 s and 18 to 21 s, respectively. The latter period refers to the duration that bubbles have reached the free surface. As seen from Figure 14a, due to the absence of buoyancy force, most bubbles are concentrated at the bottom of the column near the gas injection region. With the development of the flow, more new bubbles are injected into the bottom of the column; these new bubbles increase the liquid velocity and cause the earlier injected bubbles to

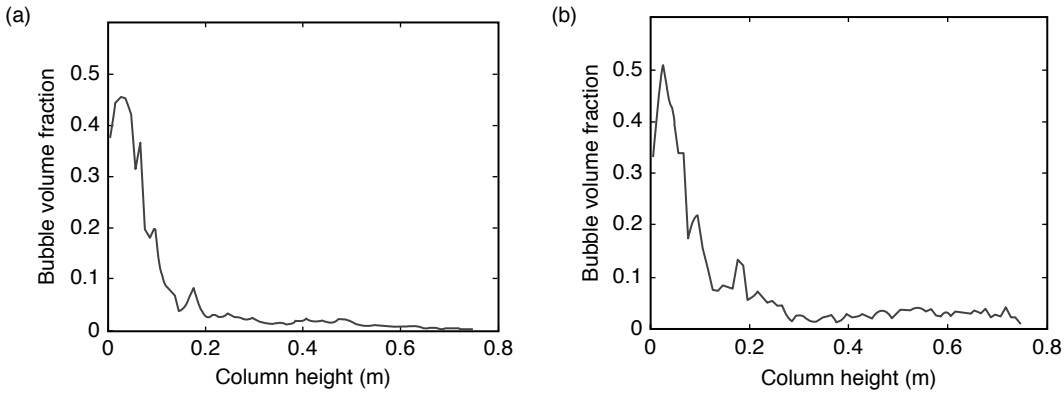


Figure 14. Average volume fraction of the bubbles along the column height in the gas-liquid-particle three-phase flow in zero-gravity. Superficial gas velocity $U_s$ = 0.25 mm/s, initial bubble size $d_b$ = 1.0 mm, particle size $d_p$= 0.25 mm. (a) Averaged over 5—20 s. (b) Averaged over 18—21 s.

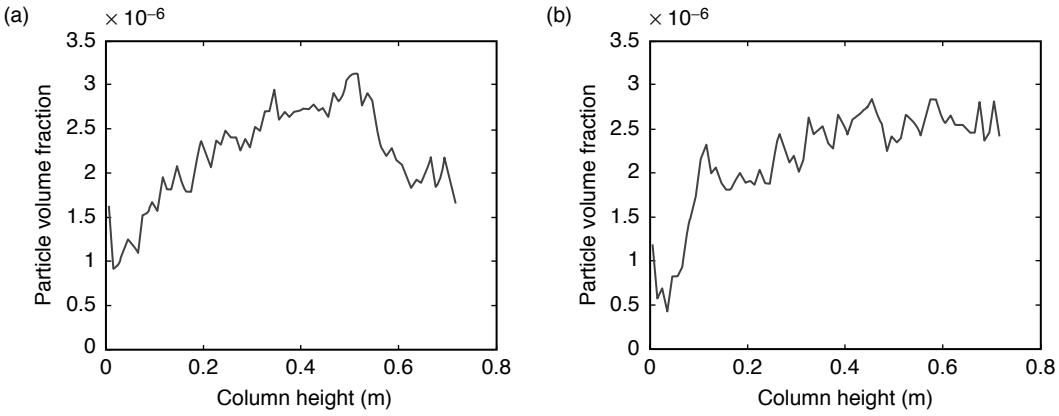


Figure 15: Average volume fraction of the particles along the column height in the gas-liquid-particle three-phase flow in zero-gravity. Superficial gas velocity $U_s$ = 0.25 mm/s, initial bubble size $d_b$ = 1.0 mm, particle size $d_p$ = 0.25 mm. a) Averaged over 5—20 s. (b) Averaged over 18—21 s.

move toward the top of the column. As a result, bubble volume fraction in the column increases with time, as seen in Figure 14.

Figure 15a shows that most particles are concentrated in the middle part of the column. The particle volume fraction is low at the lower and upper parts of the column. These low particle volume fractions are due to the gas injection in the bottom of the bubble column and the subsequent expansion of free surface in the upper part. When the bubble plume reaches the free surface, as seen from Figure 15b, particle volume fraction increases along the height of the column. Comparing Figures 15a and 15b shows that particle volume fraction at the lower part of the column decreases at the latter time, indicating that more particles are pushed away by the bubble injection. The decrease of the maximum particle volume fraction in Figure 15b is the result of the rising level of liquid in the column.

Figures 16a and 16b show the average Sauter diameter of the bubbles along the column height in the three-phase flow under zero-gravity condition over time durations of 5–20 s and 18–21 s, respectively. These figures indicate that the Sauter mean diameter of the bubbles increases along the height of the column, and the Sauter mean diameter of the bubbles in Figure16b is larger than that in Figure 16a, which means that the Sauter mean diameter of the bubbles is proportional to the residence time of the bubbles in the column. The longer the bubbles' residence time, the higher the possibility they will collide with each other and coalesce. Due to this bubble coalescence, bubble diameter not only increases along the column height, but also increases with time.

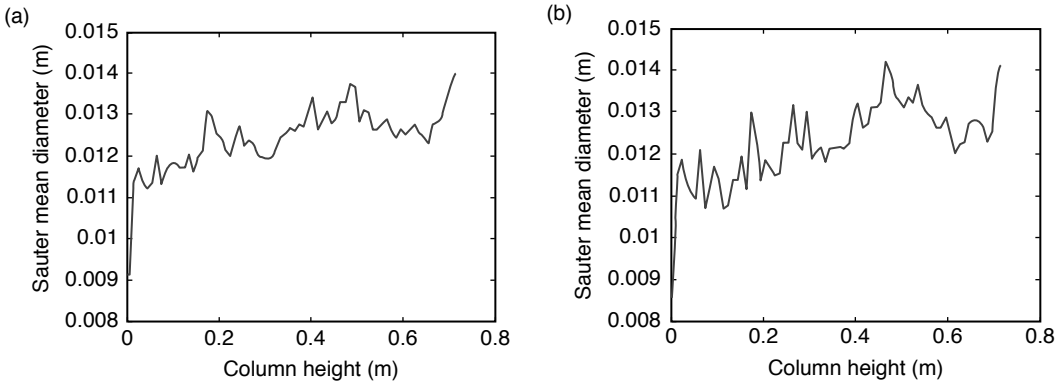


Figure 16: Average Sauter mean diameter of the bubbles along the column height in the gas-liquid-particle three-phase flow in zero-gravity. Superficial gas velocity $U_s$ = 0.25 mm/s, initial bubble size $d_b$ = 1.0 mm, particle size $d_p$ = 0.25 mm. a) Averaged over 5—20 s. (b) Averaged over 18—21 s.

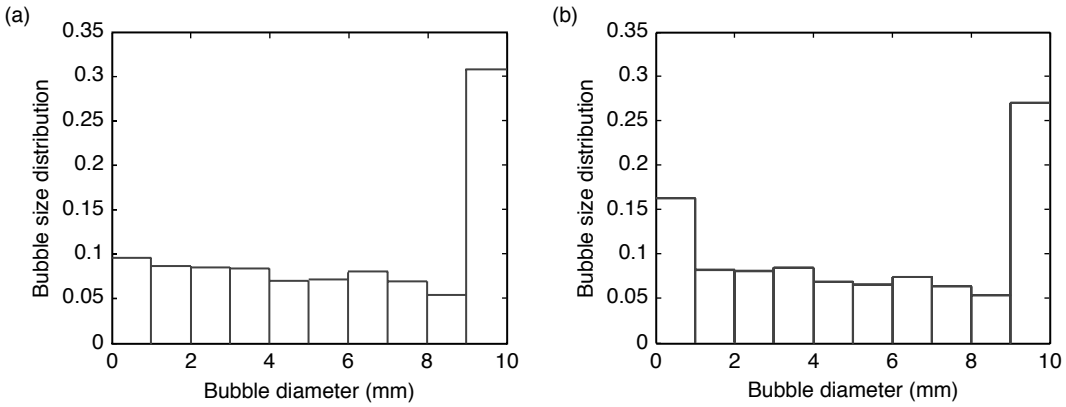


Figure 17: Bubble size distribution during gas-liquid-particle three-phase flows in zero-gravity in the entire column. Superficial gas velocity, $U_s$ = 0.25 mm/s, initial bubble size $d_b$ = 1.0 mm, particle size $d_p$ = 0.25 mm. (a) Averaged over 5—20 s. (b) Averaged over 18—21 s.

Figures 17a and 17b show average bubble size distributions in the entire column averaged over time durations of 5–20 s and 18–21 s, respectively, during three-phase flows under zero-gravity condition. As seen from Figure 17a, due to the lack of buoyancy force, the 1 mm bubbles accumulate at the bottom of the column near the injectors. Thus, bubble-bubble collisions and coalescence increase, and bubble sizes become quite large. It is seen that the number density of bubbles with a diameter larger than 9 mm is the highest. However, with the development of flow, more and more bubbles leave the bottom and rise to the middle and top of the column, so the possibility of bubble-bubble collision and coalescence at the bottom becomes relatively low. Thus the number density of large bubbles decreases and the number density of small bubbles increases, as shown in Fig 17b. Figures 17a and 17b show that bubbles with a diameter of 1 mm have the second largest amplitude in the distribution.

Compared with Figure 6, Figure 14 shows that the bubble distribution in zero-gravity is not as uniform as that in normal gravity. Similar trends are also observed for particles as shown in Figure 7 and Figure 15. These indicate again that the phase mixing in zero- gravity is not as effective as that in normal gravity. Comparison of Figures 16 and 8 shows that bubbles in zero-gravity are much larger than those in normal gravity. Compared with Figure 9, Figure 17 shows that larger bubbles are the majority. Large bubbles indicate the decrease of the contact area between bubble and liquid, suggesting that the flow in zero-gravity has low phase mixing which may result in lower chemical reaction productivity.

### 3.3. Effect of Bubble Size on Gas-Liquid-Particle Flow in Zero-gravity

To study the effect of bubble size on the flow characteristics in zero-gravity, the simulation was repeated with the inlet bubble diameter increased to 3 mm and superficial velocity increased to 6.75 mm/s, which maintained the same number of bubble injections at the inlet. Other simulation parameters are the same as those listed in Table 1 (case 3). Figure 18a shows the flow structures at 6 s after initiation of the three-phase flow. Figures 18b, c and d show the corresponding velocities of bubbles, liquid, and particles, respectively.

Compared to Figures 10a and 11a, Figures 18a and 18b show that larger bubbles have larger velocities for a fixed number of injections; thus, the bubble plume evolves faster than that with smaller inlet bubbles. Comparisons of Figure 12a and Figure 18c, as well as Figure 13a and Figure 18d, indicate that both liquid and particle velocities with larger inlet bubbles are higher than those velocities with smaller inlet bubbles. The observed trends can be explained by bubble inertia and the momentum transferred among the three phases. Since the number of injected bubbles is fixed, larger bubbles imply larger superficial velocity, which indicates that in the same time period greater bubble momentum is introduced into the column and transferred to the liquid and particle phases. Therefore, the liquid and particle velocities in the column are higher than those with smaller injected bubbles.

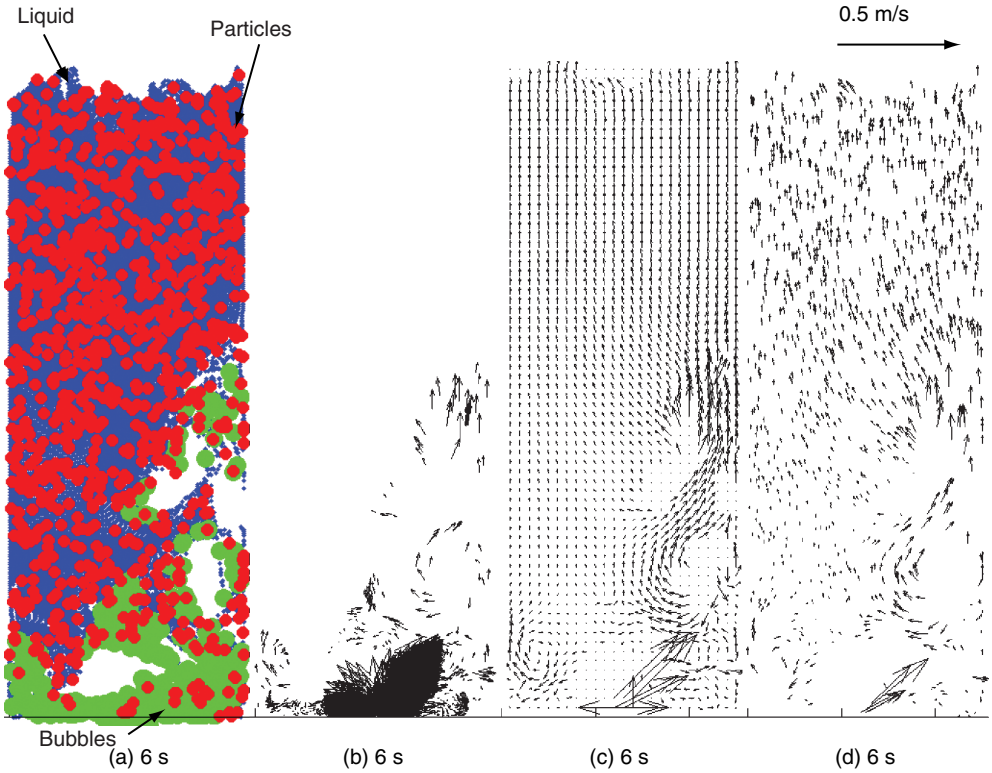


Figure 18: Computed flow structure and velocities of the gas-liquid-particle three-phase flow in zero-gravity. Superficial gas velocity $U_s$ = 6.75 mm/s, initial bubble size $d_b$ = 3.0 mm, particle size, $d_p$ = 0.25 mm.

### 3.4. Effect of g-jitter Acceleration on Gas-Liquid-Particle Flow in Zero-gravity

To study the effect of g-jitter acceleration on the gas-liquid-particle three-phase flow characteristics in zero-gravity, a simulation was performed under g-jitter acceleration from STS-51 data. The simulation parameters are listed in case 4 of Table 1. Figure 19 shows the variation of g-jitter acceleration with time from STS-51 data. It is seen from Figure 19 that g-jitter acceleration is very small compared to the acceleration of normal gravity. In the simulation, the g-jitter acceleration is used in the equation of motion of the liquid phase as body force acceleration. Figure 20a shows the flow structures at 6 s after initiation of the three-phase flow under g-jitter acceleration. Figures 20b, c and d, respectively, show the corresponding velocities of bubbles, liquid, and particles. Compared to Figure 18, Figure 20 shows a slightly more uniform bubble distribution due to the shaking effect of g-jitter acceleration, but the differences are small. This implies that the effect of g-jitter acceleration on the gas-liquid-particle three-phase flows is small.

To study more details of the effect of g-jitter, a series of comparisons are performed. Figures 21 and 22, respectively, compare the average volume fraction of the bubbles and particles along the column height over time durations of 5–6 s after initiation of the three- phase flow under g-jitter acceleration and zero-gravity. Here, a and b, respectively refer to the flow with and without g-jitter acceleration. It is seen that g-jitter leads to lower bubble volume fraction in the lower part column at the height less than 0.05 m but higher bubble volume fraction in a height of 0.05 to 0.3 m near the center of the bubble plumes. The reason is that g-jitter enhances the diffusion process and bubbles are dispersed more uniformly when compared with the absence of g-jitter. These upward moving bubbles also cause the particles in the bottom of the column to move upward to the middle of the plume. Compared to Figure 22b (absence of g-jitter), Figure 22a shows lower particle volume fraction in a height of 0.02 to 0.25 m near the lower part of the column and higher particle volume fraction in the height of 0.25 to 0.45 m on the middle of the bubble plume.

Figure 23 shows the variation of bubble Sauter mean diameters along the column height averaged over time durations of 5–6 s in the presence and absence of g-jitter. Figure 23 a shows

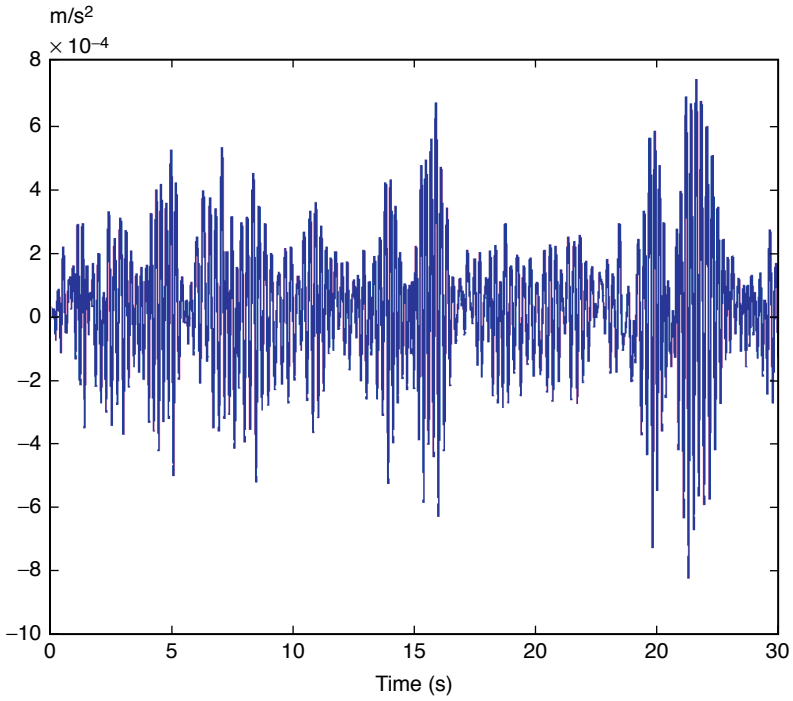


Figure 19: The variation of g-jitter acceleration with time from STS 51 data.

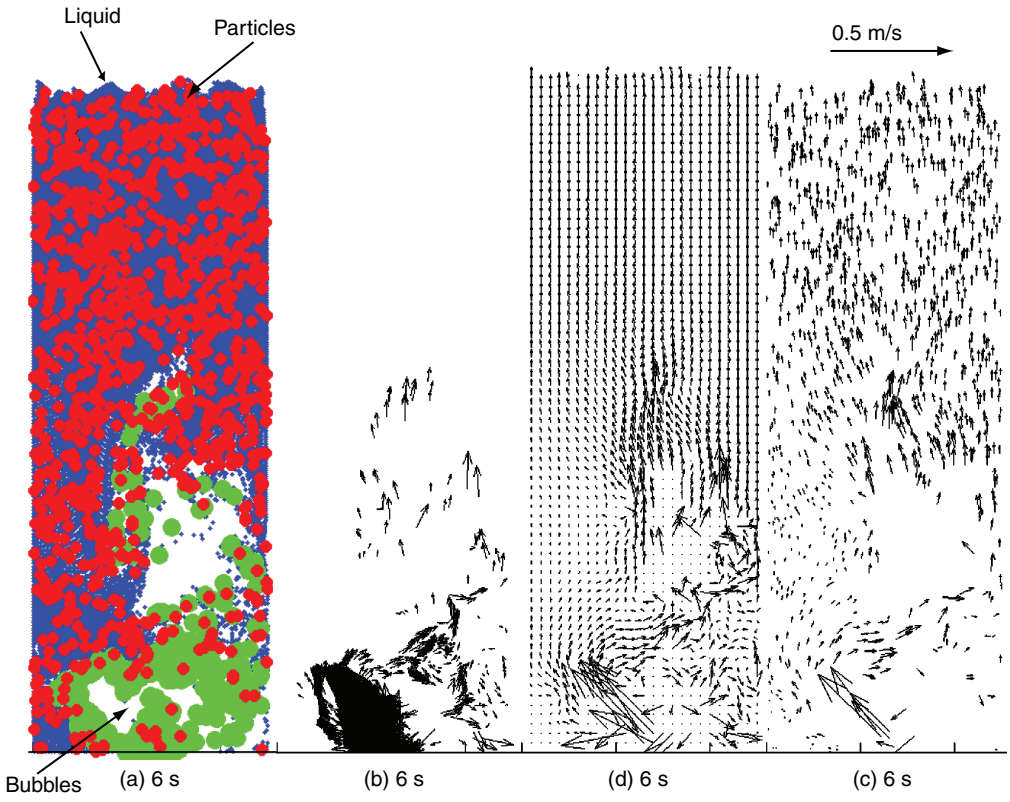


Figure 20: Computed flow structure of the gas-liquid-particle three-phase flow in zero-gravity with g-jitter. Superficial gas velocity $U_s$ = 6.75 mm/s, initial bubble size $d_b$ = 3.0 mm, particle size, $d_p$ = 0.25 mm.

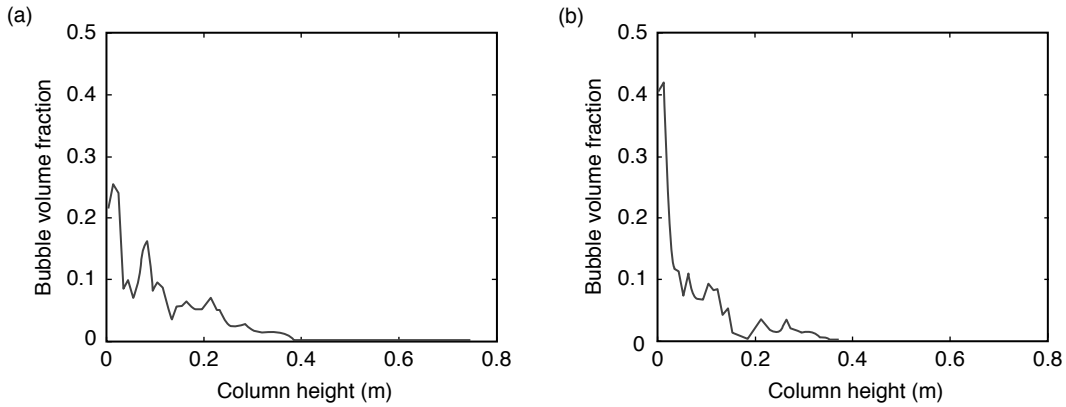


Figure 21: Average volume fraction of the bubbles along the column height over 5—6 s in the gas-liquid-particle three-phase flow. Superficial gas velocity $U_s$ = 6.75 mm/s, initial bubble size $d_b$ = 3.0 mm, particle size, $d_p$ = 0.25 mm. (a) With g-jitter. (b) Without g-jitter.

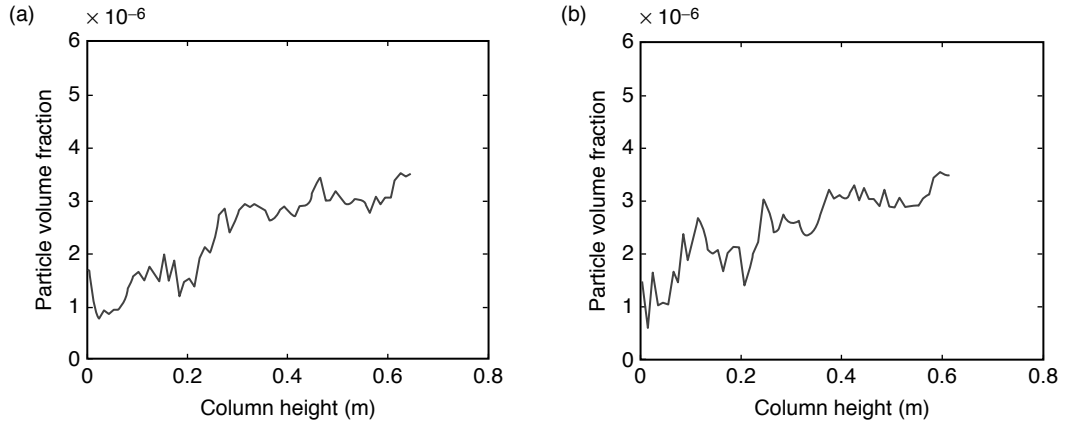


Figure 22: Average volume fraction of the particles along the column height over 5—6 s in the gas-liquid-particle three-phase flow. Superficial gas velocity $U_s$ = 6.75 mm/s, initial bubble size $d_b$ = 3.0 mm, particle size, $d_p$ = 0.25 mm. (a) With g-jitter. (b) Without g-jitter.

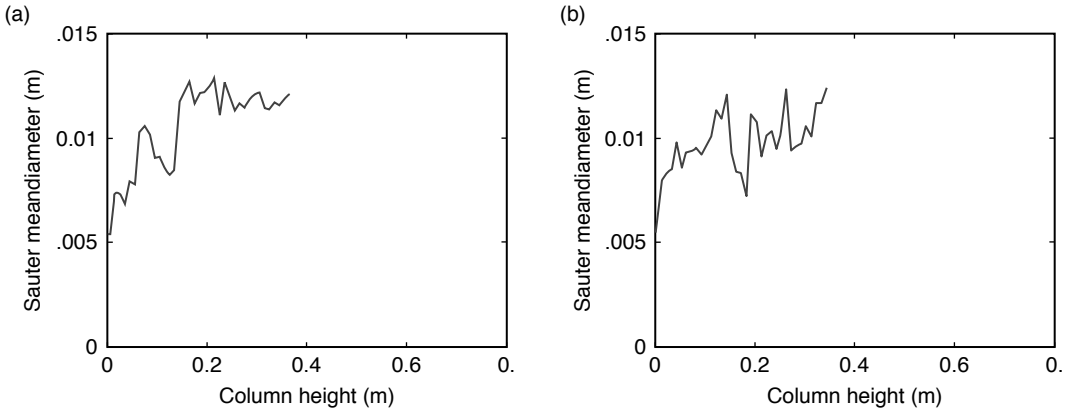


Figure 23. Average Sauter mean diameter of the bubbles along the column height over 5—6 s in the gas-liquid-particle three-phase flow. Superficial gas velocity $U_s$ = 6.75 mm/s, initial bubble size $d_b$ = 3.0 mm, particle size, $d_p$ = 0.25 mm. (a) With g-jitter. (b) Without g-jitter.

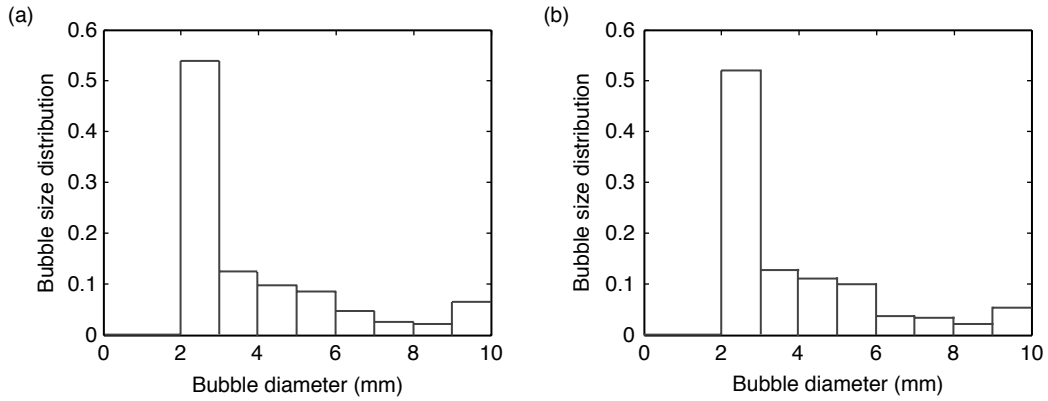


Figure 24: Bubble size distribution averaged over 5—6s during gas-liquid-particle three-phase flows in the entire column. Superficial gas velocity $U_s$ = 6.75 mm/s, initial bubble size $d_b$ = 3.0 mm, particle size, $d_p$ = 0.25 mm. (a) With g-jitter. (b) Without g-jitter.

g-jitter causes smaller bubble diameter in the lower part of the column less than 0.13 m and larger bubble diameters above 0.13 m. The reason is that the g-jitter acceleration increases bubble-bubble collision and coalescence in the middle and upper part of the plume.

Figures 24a and 24b compare bubble size distribution in the entire column in the presence and absence of g-jitter acceleration. The averaging is carried out over 5–6s. It is seen that g-jitter causes a slight increase in the number density of small 3 mm bubbles and large 9 to 11 mm bubbles, while it leads to somewhat lower number density for middle size bubbles of 3 to 9 mm.

## 4. CONCLUSIONS

In this study, an Eulerian-Lagrangian computational model for simulations of gas-liquid-solid flows in microgravity is presented. The two-way couplings between bubble-liquid and particle-liquid are accounted for in the analysis. Interactions between particle-particle and bubble-bubble are included using the hard sphere model approach, and the bubble coalescence is also included in the model. The transient characteristics of three-phase flows in zero-gravity and microgravity are studied and the effects of gravity, bubble size and g-jitter acceleration on the characteristics of the flow are discussed. On the basis of the presented results, the following conclusions are drawn:

1. Gravity has a significant influence on the transient characteristics of the flow in the bubble column. The three-phase flow in the bubble column with normal gravity is dominated by time-dependent staggered vortices; while in the flow without gravity, the sources for bubble motion are mainly bubble initial momentum, bubble-bubble collision and liquid transportation. Thus bubbles accumulate at the bottom of the column and move very slowly, and the liquid level is much higher than that of the flow with normal gravity.
2. Particles are mainly located outside the bubble plume; only a few particles are retained inside the bubble plume. The flow in zero-gravity has low phase velocities and phase mixing.
3. The velocities of bubbles, liquid and particles are in the same order.
4. After the bubble plume reaches the surface, the particle volume fraction increases along the height of the column.
5. The Sauter mean diameter of the bubbles is proportional to the transient time of the bubble; bubble diameter not only increases along the column height, but also increases with time.
6. Due to more bubble-bubble collisions and coalescence, bubbles can become very large; bubbles with a diameter larger than 9 mm have the largest amplitude in the bubble size distribution in the whole column.
7. Bubble size has a major effect on the flow. Larger bubbles have larger velocities; thus the bubble plume evolves faster than that with smaller bubbles.
8. The effect of G-jitter acceleration on the gas-liquid-particle three-phase flows is small.

**ACKNOWLEDGEMENT**
The financial support by the US Department of Energy is gratefully acknowledged.

**NOMENCLATURE**

| | |
|---|---|
| $C_D$ | drag coefficient, dimensionless |
| $d_b$ | bubble diameter, m |
| $d_p$ | particle diameter, m |
| $d_d$ | discrete phase diameter, m |
| $dt$ | minimum time for next collision, s |
| $f_d$ | coefficient used in drag coefficient calculation, dimensionless |
| $\mathbf{F_b}$ | buoyancy force, N |
| $\mathbf{F_d}$ | drag force, N |
| $\mathbf{F_{Int}}$ | Interaction force, N |
| $\mathbf{F_l}$ | Saffman force, N |
| $\mathbf{F_{vm}}$ | virtual mass force, N |
| $\mathbf{g}$ | acceleration due to gravity force, m/s$^2$ |
| $m_d$ | discrete phase mass, kg |
| $\mathbf{P}$ | momentum transferred from the discrete phase, N/kg |
| p | pressure, N/m$^2$ |
| $\mathrm{Re}_d$ | discrete phase Reynolds number, dimensionless |
| $\mathbf{u_d}$ | discrete phase velocity, m/s |
| $\mathbf{u_F}$ | fluid phase average velocity, m/s |
| $U_s$ | Superficial gas velocity |

Greek Letters

| | |
|---|---|
| $\alpha_d$ | phase coefficient, dimensionless |
| $\Delta t$ | time step for liquid phase calculation, s |
| $\varepsilon_f$ | liquid phase volume fraction, dimensionless |
| $\mu_f$ | liquid viscosity, Pa·s |
| $\rho_d$ | discrete phase density, kg/m$^3$ |
| $\rho_f$ | liquid phase density, kg/m$^3$ |
| $\tau_\mathbf{f}$ | fluid phase viscous stress tensor, N/m$^2$ |
| $\omega_\mathbf{f}$ | liquid vorticity 1/s |

**REFERENCES**

Borchers, O., Busch, C., Sokolichin, A. and Eigenberger, G., 1999. Applicability of the stand k-ε turbulence model to the dynamic simulation of bubble, Part II: Comparison of detailed experiments and flow simulations. *Chem. Eng. Sci.* **54**, pp. 5927–5935.

Bourloutski, E. and Sommerfeld M., Transient Euler/Lagrange calculations of dense gas-liquid-solid flows in bubble column with consideration of phase interaction. 2002. Proceedings 10th Workshop on Two-Phase Flow Predictions, Merseburg, pp. 113–123.

Cao, J. F., and Ahmadi, G., 1995. Gas-particle two-phase turbulent flow in a vertical duct. Int. *J. Multiphase Flow.* **21** (6), pp. 1203–1228.

Cao, J. F., and Ahmadi, G., 2000. Gas-particle two-phase turbulent flow in horizontal and inclined ducts. *Int. J. of Engineering Science* **38**, pp.1961–1981.

Delnoij, E., Kuipers, J. A. M. and van Swaaij, W. P.M., 1997a. Dynamic simulation of gas-solid two-phase flow: effect of column aspect ratio on the flow structure. *Chem. Eng. Sci.* **52**, pp. 3759–3772.

Delnoij, E., Lammers, F. A., Kuipers, J. A. M. and van Swaaij, W. P.M., 1997b. Dynamic simulation of dispersed gas-solid two-phase flow using a discrete bubble model. *Chem. Eng. Sci.* **52**, pp. 1399–1562.

Devanathan, N., Dudukovic, M. P., Lapin, A. and Lubbert, A., 1995. Chaotic flow in bubble column reactors. *Chem. Engng Sci.* **50**, pp. 2661–2667.

Ding, J. and Gidaspow, D., 1990. A bubbling fluidization model using kinetic theory of granular flow, *AICHE J.* **36**, pp. 523–538.

Fan, J., Zheng, Y., Yao, J. and Cen, K., 2001. Direct simulation of particle dispersion in a three-dimensional temporal mixing layer. Proc. R. Soc. Lond. A **457**, pp. 2151–2166.

Fan, J., Luo, K., Zheng, Y., Jin H. and Cen, K., 2003. Modulation on coherent vortex structures by dispersed solid particles in a three-dimensional mixing layer. *Physical Review E.,* **68**(3), 036309.

Fan, J., Luo, K., Ha, M. and Cen, K., 2004. Direct numerical simulation of a near-field particle-laden plane turbulent jet. *Physical Review E.,* **70**, 026303.

Fan, L.-S., 1989. Gas-Liquid-Solid Fluidization Engineering, Butterworths, Boston.

Gamwo, I.K., Halow, J.S., Gidaspow, D., and Mostofi, R., 2003. CFD Models for Methanol Synthesis Three-Phase Reactors: Reactor Optimization, Chemical Engineering Science **93**, pp. 103–112.

Gidaspow, D., Bahary, M. and Jayaswal, U. K.,1994. Hydrodynamic models for gas-liquid-solid fluidization. *Numerical Methods in Multiphase Flows,* FED **185**, ASME, New York, NY, pp. 117–124.

Grevskott, S., Sannas, B. H. , Dudukovic, M. P., Hjarbo, K. W. and Svendsen, H. F., 1996. Liquid circulation, bubble size distributions, and solids movement in two- and three-phase bubble columns, *Chem. Eng. Sci.* **51**, pp. 1703–1713.

Griebel, M., Dornseifer, T. and Neunhoeffer, T., 1998. Numerical Simulation in Fluid Dynamics: A practical introduction. The Society for Industrial and Applied Mathematics, Philadelphia, PA.

Harlow, F. and Welch, J., 1965. Numerical calculation of time-dependent viscous incompressible flow of fluid with free surface. *Phys. Fluid,* **8**, pp. 2182–2189.

Hoomans, B. P. B., Kuipers, J. A. M. and Briels, W. J., 1996. Discrete particle simulation of bubble and slug formation in a two-dimensional gas-fluidized bed: a hard-sphere approach. *Chem. Eng. Sci.* **51**, pp. 99–118.

Kvasnak, W. and Ahmadi, G., 1996. Deposition of ellipsoidal particles in turbulent duct Flows. *Chem. Eng. Sci.* **51**, pp. 5137–5148.

Krishna, R., Urseanu, M. I., van Baten, J. M., and Ellenberger, J., 1999. Influence of scale on the hydrodynamics of bubble columns operating in the churn-turbulent regime: experiments vs. Eulerian simulations. *Chem. Eng. Sci.* **54**, 4903–4911.

Lain, S., Broder, D. and Sommerfeld, M., 1999. Experimental and numerical studies of the hydrodynamics in a bubble column. *Chem. Eng. Sci.* **54**, pp. 4913–4920.

Lain, S., Broder, D., Sommerfeld, M. and Goz, M. F. 2002. Modelling hydrodynamics and turbulence in a bubble column using the Euler-Lagrange procedure. *Int. J. Multiphase Flow* **28**, pp. 1381–1407.

Lapin, A. and Lubbert, A., 1994. Numerical simulation of the dynamics of two phase gas-liquid flows in bubble columns. *Chem. Eng. Sci.* **49**, pp. 3661–3684.

Lapin, A., Paaschen, T., Junghans, K., Lubbert, A., 2002. Bubble column fluid dynamics, flow structures in slender columns with large-diameter ring-spargers. *Chem. Eng. Sci.* **57**, pp. 1419–1424.

Li, A., Ahmadi, G., Bayer, R.G. and Gaynes, M.A., 1994. Aerosols Particle Deposition in an Obstructed Turbulent Duct Flow, *J. Aerosol Science,* **2**5, pp. 91–112.

Mansoori, Z., Saffar-Avval, M., Basirat Tabrizi, H and Ahmadi, G., 2002a. Modeling of Heat Transfer in Turbulent Gas-Solid Flow, *International Journal Heat Mass and Transfer,* **45**, pp. 1173–1184.

Mansoori, Z., Saffar-Avval, M., Basirat Tabrizi, H., Ahmadi, G., and Lain. S., 2002b. Thermo-Mechanical Modeling of Turbulent Heat Transfer in Gas-Solid Flows Including Particle Collisions, *International Journal of Heat and Fluid Flow,* **23**, pp. 792–806.

Mitra-Majumdar, D., Farouk, B. and Shah, Y. T., 1997. Hydrodynamic modeling of three-phase flows through a vertical column. *Chem. Eng. Sci.* **52**, pp. 4485–4497.

Mudde, R. F., and Simonin, O., 1999. Two- and three-dimensional simulations of a bubble plume using a two-fluid model. *Chem. Eng. Sci.* **54**, pp. 5061–5069.

Padial, N. T., Vander Heyden, W. B., Rauenzahn, R. M. and Yarbo, S. L., 2000. Three-Dimensional simulation of a three-phase draft-tube bubble column. *Chem. Eng. Sci.* **55**, 3261–3273.

Patankar, N. A. and Joseph, D. D., 2001a. Modeling and numerical simulation of particulate flows by the Eulerian-Lagrangian approach. *Int. J. Multiphase Flow* **27**, pp. 1659–1684.

Patankar, N. A. and Joseph, D. D., 2001b, Lagrangian numerical simulation of particulate Flows. *Int. J. Multiphase Flow* **27**, pp. 1685–1706.

Pita, J. A. and Sandaresan, S., 1993. Developing flow of a gas-particle mixture in a vertical riser, *AICHE* J. **39**, pp. 541–552.

Sanyal, J., Vasquez, S., Roy, S., and Dudukovic, M. P., 1999. Numerical simulation of gas-liquid dynamics in cylindrical bubble column reactors. *Chem. Eng. Sci.* **54**, pp. 5071–5083.

Sokolichin, A. and Eigenberger, G., Lapin, A., Lubert, A., 1997. Dynamic numerical simulation of gas-liquid two-phase flows Euler/Euler versus Euler/Lagrange. *Chem. Eng. Sci.* **52**, pp. 611–626.

Trapp, J. A. and Mortensen, G. A., 1993. A discrete particle model for bubble slug two phase flow. *J. Comp. Phys.* **107**, pp. 367–377.

Tsuji, Y., Kawaguchi, T. and Tanaka, T., 1993. Discrete particle simulation of two dimensional fluidized bed. *Powder Technol.* **77**, pp. 79–87.

Webb, C., Que, F. and Senior, P. R., 1992. Dynamic simulation of gas-liquid dispersion behavior in a 2-D bubble column using a graphics mini-supercomputer. *Chem. Eng. Sci.* **47**, pp. 3305–3312.

Wu, Y., Gidaspow, D., 2000. Hydrodynamic simulation of methanol synthesis in gas-liquid slurry bubble column reactors. *Chem. Eng. Sci.* **55**, pp. 573–587.

Xu, B. H. and Yu, A. B., 1997. Numerical simulation of the gas-solid flow in a fluidized bed by combing discrete particle method with computational fluid dynamics. *Chem. Eng. Sci.* **52**, pp. 2785–2809.

Zhang, J. P, 1999. Discrete phase simulation of bubble and particle dynamics in gas-liquid-solid fluidization systems. Ph.D. thesis, The Ohio State University.

Zhang, X., 1998, Study of gas-solid multiphase flow characteristics in impact rich/lean burners and curved ducts, Ph.D. dissertation, Zhejiang University, Hangzhou, Zhejiang, P. R. China.

Zhang, X. and Ahmadi, G., 2005. Eulerian-Lagrangian simulations of liquid-gas-solid flows in three-phase slurry reactors. *Chem. Eng. Sci.* **60**, pp. 5089–5104.

Zhou, L., Yang, M. and Fan L., 2005. A second-order moment three-phase turbulence model for simulating gas-liquid-solid flows. *Chem. Eng. Sci.* **60**, pp. 647–653.